

Changes in regional lung mechanics and ventilation distribution after unilateral pulmonary artery occlusion

BRETT A. SIMON,² KOICHI TSUZAKI,¹ AND JOSE G. VENEGAS¹

¹Departments of Anesthesia and Biomedical Engineering, Massachusetts General Hospital, Harvard Medical School, Boston, Massachusetts 02114; ²Department of Anesthesia and Critical Care Medicine, Johns Hopkins Medical Institutions, Baltimore, Maryland 21287-8711

Simon, Brett A., Koichi Tsuzaki, and Jose G. Venegas.

Changes in regional lung mechanics and ventilation distribution after unilateral pulmonary artery occlusion. *J. Appl. Physiol.* 82(3): 882–891, 1997.—Regional pneumoconstriction induced by alveolar hypocapnia is an important homeostatic mechanism for optimization of ventilation-perfusion matching. We used positron imaging of ¹³NN-equilibrated lungs to measure the distribution of regional tidal volume (V_T), lung volume (V_L), and lung impedance (Z) before and after left (L) pulmonary artery occlusion (PAO) in eight anesthetized, open-chest dogs. Measurements were made during eupapnic sinusoidal ventilation at 0.2 Hz with 4-cmH₂O positive end expiratory pressure. Right (R) and L lung impedances (Z_R and Z_L) were determined from carinal pressure and positron imaging of dynamic regional V_L. LPAO caused an increase in |Z_L| relative to |Z_R|, resulting in a shift in V_T away from the PAO side, with a L/R |Z| ratio changing from 1.20 ± 0.07 (mean ± SE) to 2.79 ± 0.85 after LPAO (P < 0.05). Although mean L lung V_L decreased slightly, the V_L normalized parameters specific admittance and specific compliance both significantly decreased with PAO. Lung recoil pressure at 50% total lung capacity also increased after PAO. We conclude that PAO results in an increase in regional lung Z that shifts ventilation away from the affected area at normal breathing frequencies and that this effect is not due to a change in V_L but reflects mechanical constriction at the tissue level.

positron imaging; lung impedance; dogs; hypocapnia; compliance

REGIONAL PNEUMOCONSTRICTION induced by alveolar hypocapnia has been proposed as a homeostatic mechanism for optimization of ventilation-perfusion matching. Severinghaus et al (12) showed that unilateral pulmonary artery occlusion (PAO) caused an increase in lung resistance and decrease in compliance associated with a shift in regional tidal volume (V_{T,r}) away from the occluded side. This effect was prevented by the inhalation of CO₂. Similarly, Ingram (4) demonstrated that alveolar hypocapnia, with unilateral PAO and systemic normocapnia, caused greatly increased lung resistance and decreased compliance. Presumably, this mechanism serves to shunt alveolar ventilation away from hypoperfused lung regions for optimizing of ventilation-perfusion matching—the airways counterpart to hypoxic pulmonary vasoconstriction.

In a preliminary study, we showed that alveolar hypocapnia, with normal systemic blood gases achieved by using extra-corporeal membrane oxygenation (ECMO), caused an increase in both the real (Re) and imaginary (Im) parts of whole lung impedance (Z) over the frequency range 0.5–15 Hz (24). This effect was greater at lower frequencies, suggesting an important

role for tissue properties. To further explore this phenomenon and its role in redistributing ventilation, we used dynamic positron imaging with radioactive ¹³NN gas (16, 22, 23) to measure the distribution of V_{T,r}, regional lung volume (V_{L,r}), and regional lung Z (Z_r) at 0.2 Hz before and after left (L) PAO in anesthetized, open-chest dogs. This technique allowed the direct measurement of V_{L,r} and input Z during nonhomogeneous interventions, such as unilateral PAO, with airflow and volume distribution according to regional mechanical properties. Furthermore, the effects of PAO on ventilatory heterogeneity were assessed by examination of the regional tracer-washout curves, and gas trapping was assessed by comparison of the volume of tracer gas present after equilibration of the lung during ventilation with normal V_T with that equilibrated with several breaths to total lung capacity (TLC). Finally, lung recoil was quantified by examination of regional in situ deflation pressure-volume (P-V) curves of the individual lungs.

MATERIALS AND METHODS

Experimental preparation. All protocols and procedures were approved by the animal care committee of the Massachusetts General Hospital. Eight mongrel dogs weighing between 12.5 and 15 kg (mean body weight = 13.9 kg) were anesthetized with an intravenous bolus of pentobarbital sodium (25 mg/kg) and fentanyl citrate (50 μg/kg), and maintained with a continuous infusion of α-chloralose (80–100 mg/kg bolus, 80 mg·kg⁻¹·h⁻¹ infusion). Additional fentanyl citrate (25–50 μg/kg) was given at the start of the imaging studies. Femoral arterial and venous catheters were placed for arterial pressure monitoring, blood-gas sampling, and administering of fluid and drugs. A tracheotomy was performed, and a cuffed endotracheal tube (10-mm ID, 12-cm length) was secured into place in the midtrachea. Catheters were placed in the distal trachea for measurement of carinal pressure (P_{ca}) and delivery of bias flow. The chest was opened wide via a median sternotomy and retraction of the abdominal viscera. The left pulmonary artery (Lpa) was isolated within the pericardium, and an umbilical tape occluder was placed loosely around the Lpa. The exposed lungs and viscera were covered with saline-moistened gauze sponges and plastic wrap to prevent drying, and the animals were positioned supine between the opposing planar array of detectors of a positron camera. Animal position was fixed by gentle limb traction. A water-filled warming pad and radiant heat lamp were used to maintain rectal temperature at 36 ± 1°C.

Mechanical ventilation was provided via a closed-loop rebreathing circuit including a linear motor driven piston oscillator, a bell spirometer, a CO₂ absorber, a bias flow of 20 l/min, and supplemental oxygen. The piston pump (14) was used for both conventional and high-frequency oscillatory ventilation (HFV) and was sinusoidally driven by a function generator (model 85, Wavetek, San Diego, CA). V_T was

adjusted to provide eucapnic ventilation at 0.2 Hz under control conditions, as indicated by arterial blood gases, and then maintained during PAO. Mean airway pressure (P_{aw}) was measured from a small-diameter flush sidearm on a rigid Plexiglas tube (27-cm long, 2.54-cm ID) connecting the ventilator piston to the endotracheal tube (18). The bias flow was driven by a double-piston gas compressor, with one of the pistons used to force the bias flow through the side holes of a 1-mm ID catheter positioned at the distal end of the endotracheal tube. The second piston was used to suction the gas from the oscillator end of the Plexiglas connecting tube via a high-Z orifice. A pneumatic feedback-controlled vacuum regulator was used to vary the outflow resistance to regulate the \bar{P}_{aw} , which was set to 4 cmH₂O positive end expiratory pressure. Solenoid valves allowed the rapid switching of bias flow composition between the closed-loop breathing circuit and fresh air.

Oscillatory flow was measured with a screen pneumotachograph (Erich Jaeger, Höchberg, Germany) and a differential-pressure transducer (MP-45, Validyne Engineering, Northridge, CA). The frequency response of this system was found to be flat up to 30 Hz. Pca was measured with a solid-state pressure transducer (Gould TC-DT-16) through the side ports of a 30-cm long, 2-mm ID air-filled catheter placed at the carina by fiberoptic bronchoscopy. Pressure, flow, and a ventilator sync signal were acquired on a Compaq Portable II computer equipped with a data acquisition board (DT2801-A, Data Translation, Marlboro, MA) and dedicated software written with the use of the ASYST package (Asyst Software Technologies, Rochester, NY). The total V_T delivered was calculated on-line by numerical integration of the oscillatory flow signal.

Positron imaging. Dynamic V_{Lr} and gas transport were assessed by using a two-dimensional planar positron camera that recorded the radioactive decay events of the short-lived positron emitter ¹³NN ($t_{1/2} = 9.96$ min) as a matrix of 64×64 pixels (1). The camera's digital electronics were modified to allow collection of multiple-gated sequential images as short as 5 ms each. The imaging techniques used for dynamic V_{Lr} and lung Zr measurements have been described in detail previously (22, 23), and the basic procedure is briefly described below. An imaging run started with the introduction of a bolus of ¹³NN (~40 mCi) into the closed rebreathing circuit during steady-state ventilation. Once equilibration with the lungs was established, a respiratory-gating protocol was used to measure dynamic V_{Lr} and V_{Tr} . Each image was sampled over a period of 0.5 s so that the series of 15 images covered exactly one and one-half breathing cycles. Collection of this image was triggered by a signal from the function generator that also served to drive the ventilator and trigger the acquisition of the pressure and flow signals. The gated imaging was continued for a total collection time of 6 min, divided into consecutive segments of 1, 3, and 2 min, typically resulting in at least 300,000 counts per image. The shorter first and third segments of these consecutive-image collections were performed to assess the stability of the measurements over the measurement period, whereas the longer middle segment of data was used for the Z analysis. Finally, a washout maneuver was performed to measure regional gas transport. This consisted of an equilibration image of 60-s duration, after which the bias flow was switched to unlabeled fresh air, and thirty 5-s serial images of the lung washout of ¹³NN were obtained.

Image analysis. Images consisted of a two-dimensional anterior-posterior projection of the lungs in which the entire lung fields were visible (22, 23). Two regions of interest were defined, separating and enclosing the L and right (R) lungs,

by using the equilibration image as a template. This image represents the mean V_L (\bar{V}_L) averaged over many breaths at constant V_T and ensures that the regions of interest entirely enclose each lung throughout the respiratory cycle. Care was taken to exclude from the L lung region that portion of the R-sided cardiac lobe which sometimes extends into the L hemithorax. A third region was selected outside the lung fields for background activity correction.

As described previously (22), the gated image series was used to determine dynamic V_{Lr} . Regional (L and R) and total number of counts $N(t)$ were expressed as a function of time and curve-fitted to the sinusoidal function

$$N(t) = \bar{N} + \frac{\Delta N}{2} \sin(\omega t + \phi) \quad (1)$$

where ω is the angular frequency ($2\pi f$), ϕ is the phase angle in radians relative to the gating signal, \bar{N} is the mean number of counts, and $\Delta N/2$ is the amplitude of oscillation. Because ¹³NN is extremely insoluble and therefore present predominantly in ventilated air spaces, in the steady state, the total and regional count rates measured by the camera should be proportional to the corresponding total and regional volumes of ventilated, air-filled lung. The value of ΔN , taken for the total lung, represents the overall lung V_T measured with the pneumotachograph. This result was used to determine a proportionality factor between counts and volume, $k = V_T/\Delta N$, which was then used to calculate total \bar{V}_L and regional mean (\bar{V}_L) and tidal (V_{Tr}) volumes

$$\begin{aligned} \bar{V}_L &= k \bar{N} \\ \bar{V}_R &= k \bar{N}_R \\ V_{Tr} &= k \Delta N_r \end{aligned} \quad (2)$$

Air trapping was assessed by comparing the \bar{V}_L measured after ¹³NN equilibration performed with TLC breaths vs. that obtained after equilibration during mechanical ventilation with normal V_T .

Regional impedance. Zr was assessed from simultaneous measurements of Pca and V_{Tr} (22). All phases were initially referenced to a sync signal from the oscillator. The amplitude and phase of the Pca ($|P_{ca}|$ and ϕ_p) were determined by curve fitting a sinusoidal function to the acquired pressure data. Amplitude and phase of regional flow ($|V_r|$ and ϕ_{V_r}) were obtained by differentiation of the fitted dynamic V_{Lr} signal (Eq. 1) determined from the gated study. Phase lags in these imaged V_{Lr} data due to time delays in data handling by the computers were estimated by comparing the phase of the overall V_L signal, measured by the pneumotachograph, to that determined by the camera from the total lung field. These results were used to reconcile the image-derived volume and flow-phase angles.

The magnitudes of the regional lung impedances ($|Z_r|$), as seen from the carina, were calculated by taking the ratio of $|P_{ca}|$ and the corresponding $|V_r|$. Similarly, the phase angle of the Z was determined by subtracting the ϕ of the regional flow and Pca

$$|Z_r| = |P_{ca}|/|V_r| \quad (3)$$

$$\phi_{Zr} = \phi_p - \phi_r \quad (4)$$

The regional lung elastance (E) [$E_r = -\omega \text{Im}[Z_r]$] and resistance [$R_r = \text{Re}[Z_r]$], where Im is imaginary and Re is real,

were calculated as

$$E_r = -\omega |Z_r| \sin(\phi_{Z_r}) \tag{5}$$

$$R_r = |Z_r| \cos(\phi_{Z_r}) \tag{6}$$

because the effects of inertia are negligible at this frequency.

Washouts. Washout curves were analyzed to estimate the presence of ventilatory heterogeneity within the whole L or R lung regions of interest. The log-transformed total counts during the washout, normalized by the equilibration counts, were plotted vs. time and fitted to a linear model. Departures from linearity of the fit indicate ventilatory heterogeneity, and the correlation coefficient (r^2) of the fit correlates with the coefficient of variation (CV) of the distribution of specific ventilations of a simple multicompartment model (see APPENDIX 1). Two washouts each (after both TLC and tidal equilibrations) for control and LPAO₁ conditions were analyzed (see *Experimental protocol*).

P-V curves. R and L lung deflation P-V curves were simultaneously obtained by imaging the ¹³NN-equilibrated lungs while stepping down from P_{aw} ~25 cmH₂O to P_{aw} = 0 in ten 10-s steps with a Plexiglas supersyringe. Individual V_L were obtained from the images as described above and plotted against the measured pressure at each step. The P-V curves were fitted to a sigmoidal equation (see APPENDIX 2), normalized to TLC (upper asymptote from the fit), and replotted. This procedure permitted differences in recoil pressure between L vs. R lungs and between control vs. PAO conditions to be quantified at a V_L of 50% of TLC.

Statistical analysis. Results were analyzed by using Student's *t*-test for paired data or the paired sign test (StatView IV, Abacus Concepts). Ratio data were log transformed, and differences with *P* values <0.05 were taken to be statistically significant.

Experimental protocol. The experimental protocol is schematically illustrated in Fig. 1. The basic process was to measure V_{Lr}, V_{Tr}, and Z_r by using the gated-image technique described above after achieving equilibration of the lungs with ¹³NN with the use of either several inflations to TLC, defined as V_L at P_{aw} = 30 cmH₂O, or mechanical ventilation with a normal V_T (tidal equilibration). With TLC equilibration, we assume that all alveoli will open and thus contain tracer gas, whereas equilibration with tidal breathing will label only normally ventilated lung regions.

Two sets of control measurements were obtained, after TLC and then tidal-breathing equilibrations (Fig. 1). An image of residual tracer was obtained before each equilibration. Next, the lungs were again equilibrated with TLC inflations, and the Lpa was then occluded by tightening the previously placed umbilical tape. In pilot studies, we confirmed complete LPAO under these conditions by imaging the lungs during a right atrial injection of dissolved ¹³NN and

verifying that no tracer showed up in the L lung for 1 min. Then, 5 min after PAO, the gated-imaging protocol was performed and also repeated after tracer washout and reequilibration with tidal breathing (LPAO₁). Without releasing the pulmonary artery occluder, a full second set of TLC and tidal breathing equilibrated measurements were then obtained (LPAO₂). Finally, deflation P-V curves were obtained as described above.

In two animals, the left pulmonary artery was inadvertently punctured during the dissection and had to be immediately clamped; thus, no control data are available for those dogs. These animals were excluded from the Z analysis but were included in the P-V analysis. Additionally, control P-V curves were also obtained in three dogs.

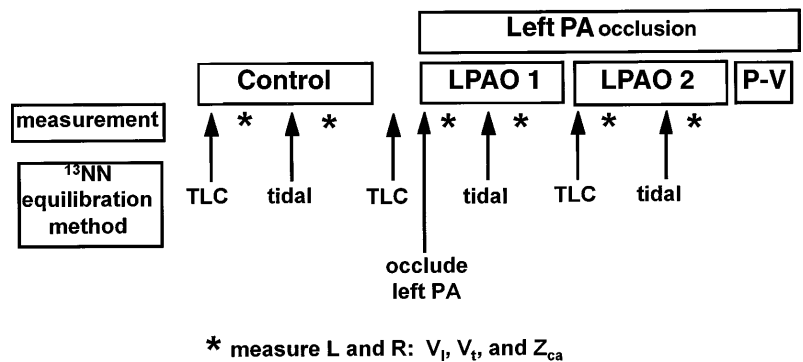
RESULTS

There were no differences in |Z| measured over the three consecutive gated-data acquisitions during each of the control, LPAO₁, and LPAO₂ measurements, indicating that the preparation was stable over the measurement period. All subsequent results refer to measurements taken during the longer, middle data acquisition that was used for further analysis because the longer acquisition provided higher counts and thus superior signal-to-noise ratio (22). Furthermore, there were no differences in |Z| for the L or R lung or the L/R |Z| ratio between the LPAO₁ and LPAO₂ measurements. Finally, there were no differences in |Z| measurements between the gated measurements taken after TLC equilibration vs. tidal equilibration for either control, LPAO₁, or LPAO₂. Further discussion refers to Z data taken from the initial (TLC-equilibrated) gated measurement from LPAO₁ unless otherwise specified.

LPAO caused a significant increase in the magnitude of left lung impedance (|Z_L|) relative to the magnitude of right lung impedance (|Z_R|), with a resultant shift in delivered V_T away from the PAO side (Fig. 2 and Table 1). The L/R |Z| ratio increased from a control value of 1.20 ± 0.07 (mean ± SE) to 2.79 ± 0.85 after LPAO (*P* < 0.05). This change in |Z| was due to increases in both L-sided Re|Z| (395%) and Im|Z| (184%), while R-side values were unchanged (Fig. 3 and Table 1). Despite this 230% increase in |Z_r| ratio, the phase difference between the lungs changed only from -0.34 ± 0.85 to 10.1 ± 0.6° (*P* < 0.001), with the obstructed L lung lagging (Fig. 2).

L/R V_T ratio decreased with LPAO from 0.85 ± 0.05 to 0.47 ± 0.08 (*P* < 0.02), as expected from the |Z|

Fig. 1. Experimental protocol. See text for details. TLC, total lung capacity; PA, pulmonary artery; LPAO, left pulmonary arterial occlusion; P-V, pressure-volume; L, left; R, right; V_L, lung volume (V_L); V_T, tidal volume (V_T); Z_{ca}, carinal impedance.



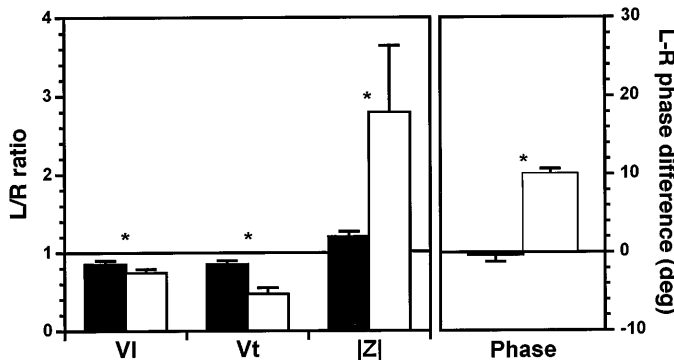


Fig. 2. Changes in L-to-R ratio of mean V_L , V_T , impedance magnitude ($|Z|$), and L-R phase difference from control (solid bars) to LPAO conditions (open bars); means \pm SE. * $P < 0.05$, control vs. LPAO.

changes. This change was due to a redistribution of V_T from the L to R lung (Table 1). L \bar{V}_L decreased slightly relative to R, resulting in a L/R V_L ratio change from 0.85 ± 0.05 to 0.74 ± 0.05 ($P < 0.01$; Fig. 2 and Table 1). However, these V_L changes per se cannot account for the observed changes in mechanical properties, because the parameters specific admittance [$sA = (|Z| \cdot V_L)^{-1}$] and specific compliance [$sC = -(\omega \cdot \text{Im}[Z] \cdot V_L)^{-1}$], which are normalized for ventilated V_L , changed significantly in the L lung (Table 1). L/R sA fell from 1.00 ± 0.06 to 0.64 ± 0.10 ($P = 0.04$) and L/R sC fell from 1.00 ± 0.06 to 0.72 ± 0.10 after LPAO ($P < 0.04$). Another intensive tissue parameter, hysteresivity (η), estimated as $\eta = -\text{Re}[Z]/\text{Im}[Z]$, also increased in the L lung relative to the R. L/R η ratio increased from 0.98 ± 0.08 to 2.04 ± 0.12 after LPAO ($P < 0.001$).

The degree of air trapping was assessed by the percent increase in \bar{V}_L measured after tracer equilibration with several inflations to TLC over that obtained after tracer equilibration with tidal breathing. The degree of air trapping was highly variable among animals, but it tended to increase in the L lung after LPAO and in both lungs over time (Fig. 4). These increases in trapped volume attained statistical significance only during LPAO₂ ($P < 0.05$) and were significant for both R and L lungs.

The deflation P-V curves showed several interesting features (Figs. 5 and 6). Curves were plotted as normalized V_L (%TLC) vs. P_{aw} to facilitate comparisons among different animals and conditions (see APPENDIX

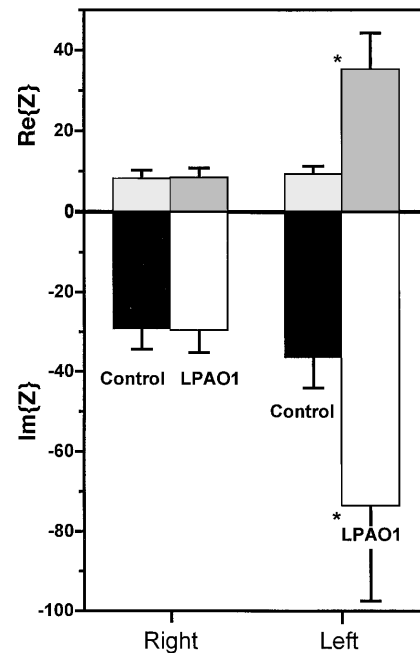


Fig. 3. Individual L and R lung complex Z components at 0.2 Hz under control and LPAO conditions; means \pm SE in $\text{cmH}_2\text{O} \cdot \text{s} \cdot \text{l}^{-1}$. * $P < 0.05$ control vs. LPAO. Re, real; Im, imaginary.

2). In all three animals in which both control and LPAO P-V curves were obtained, there was a rightward shift in the L-lung curve relative to the R lung after LPAO. Mean recoil pressure difference between L and R lungs at 50% TLC increased from 0.15 ± 0.98 to 1.54 ± 0.62 cmH_2O . Although statistical comparison between control and PAO recoil pressure was not possible because of the small sample size, it was possible to compare L and R lung recoil after LPAO. The mean L/R recoil difference at 50% TLC for all dogs after LPAO was 1.29 ± 0.28 cmH_2O ($P < 0.01$). Air trapping, manifested as the L deflation curve crossing over the R and flattening at low P_{aw} , is evident in five of the eight animals after LPAO (Figs. 5 and 6).

The linearity of the individual L and R lung log-washout curves was analyzed to assess the presence of ventilatory heterogeneity (APPENDIX 1). Departures from linearity of these whole lung log-washout curves indicate the presence of multiple parallel compartments contributing to the whole lung washout. The r^2 for the

Table 1. Gated analysis results

	Control			LPAO ₁		
	Left	Right	L/R	Left	Right	L/R
V_T , ml	76.8 ± 6.5	89.1 ± 3.3	0.85 ± 0.05	$55.2 \pm 7.7^*$	$123.0 \pm 8.6^*$	$0.47 \pm 0.08^*$
V_L , ml	329 ± 53	393 ± 61	0.85 ± 0.05	294 ± 41	412 ± 69	$0.74 \pm 0.05^*$
$ Z $, $\text{cmH}_2\text{O} \cdot \text{s} \cdot \text{l}^{-1}$	38.5 ± 6.9	31.3 ± 4.3	1.20 ± 0.07	$85.5 \pm 25.1^*$	32.0 ± 4.8	$2.79 \pm 0.85^*$
$\text{Re}[Z]$, $\text{cmH}_2\text{O} \cdot \text{s} \cdot \text{l}^{-1}$	9.3 ± 2.0	8.2 ± 2.0	1.20 ± 0.14	$35.3 \pm 8.9^*$	8.4 ± 2.4	$5.57 \pm 2.37^*$
$\text{Im}[Z]$, $\text{cmH}_2\text{O} \cdot \text{s} \cdot \text{l}^{-1}$	-36.4 ± 7.7	-29.2 ± 5.2	1.20 ± 0.06	$-73.5 \pm 26.1^*$	-29.6 ± 5.7	$2.50 \pm 0.84^*$
sA , $(\text{cmH}_2\text{O} \cdot \text{s})^{-1} (\times 100)$	10.1 ± 1.7	10.5 ± 2.2	1.00 ± 0.06	$6.0 \pm 1.3^*$	9.1 ± 1.4	$0.64 \pm 0.10^*$
sC , $(\text{cmH}_2\text{O})^{-1}$	0.09 ± 0.02	0.09 ± 0.02	1.00 ± 0.06	$0.06 \pm 0.02^*$	0.09 ± 0.02	$0.72 \pm 0.10^*$
η	0.42 ± 0.23	0.43 ± 0.24	0.98 ± 0.08	$0.87 \pm 0.51^*$	0.46 ± 0.28	$2.04 \pm 0.12^*$

Values are means \pm SE; $n = 6$. LPAO₁, first left pulmonary artery occlusion; L/R, left-to-right ratio; V_T , tidal volume; V_L , lung volume; Z , impedance; Re, real; Im, imaginary; sA , specific admittance; sC , specific compliance; η , hysteresivity. * $P < 0.05$ vs. control.

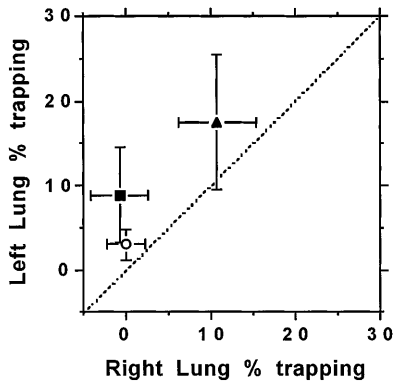


Fig. 4. Gas trapping (in %) in R vs. L lungs under control (○), LPAO₁ (■), and LPAO₂ (▲) conditions; means ± SE. See text for details.

fit of both control and LPAO log washouts to a linear model was very high, corresponding to CV of regional ventilation of <15% (Table 2). There were no significant differences between L and R or control and LPAO r^2 values.

DISCUSSION

In these studies, we have shown that LPAO with continued ventilation induces ipsilateral pneumoconstriction which, in turn, results in a redistribution of ventilation away from the hypoperfused side. Low-frequency Z measurements show increases in both the Re (related to resistance) and Im (related to E) components, although the redistribution of ventilation is primarily the result of the changes in E_r . These findings are not accounted for by changes in ventilated V_L , since sC and sA both fall in the L lung. Combined with the increase in L-lung recoil after LPAO measured from the P-V curves, these results suggest a response dominated by changes in tissue properties.

The effect of alveolar PCO_2 has long been known to be important in regional lung mechanical changes. Prompted by work performed in the 1930s through 1950s suggesting that temporary unilateral PAO did not cause the expected increases in alveolar dead space and arterial PCO_2 , Severinghaus et al. (12) demon-

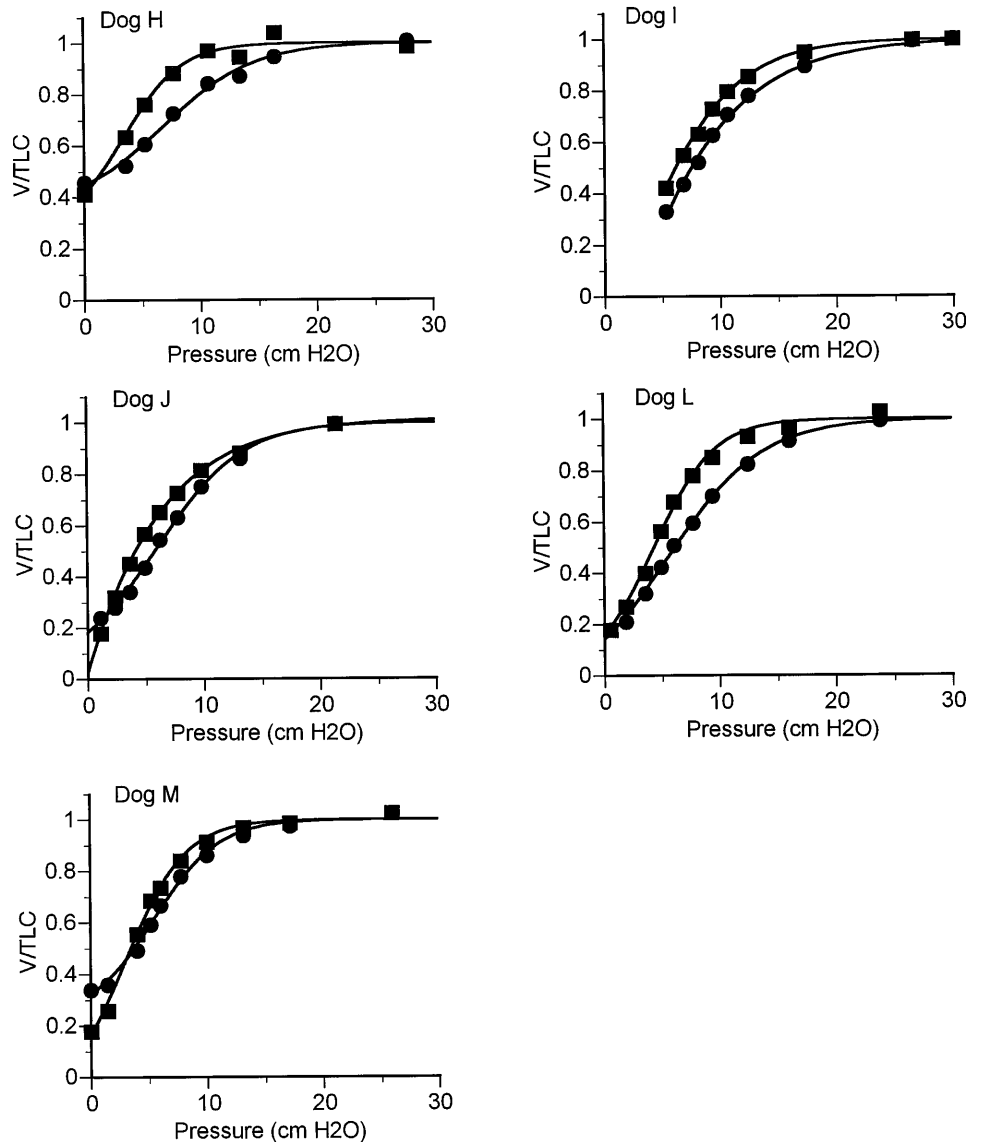


Fig. 5. Individual L (●) and R (■) lung-deflation P-V curves in 5 animals after LPAO.

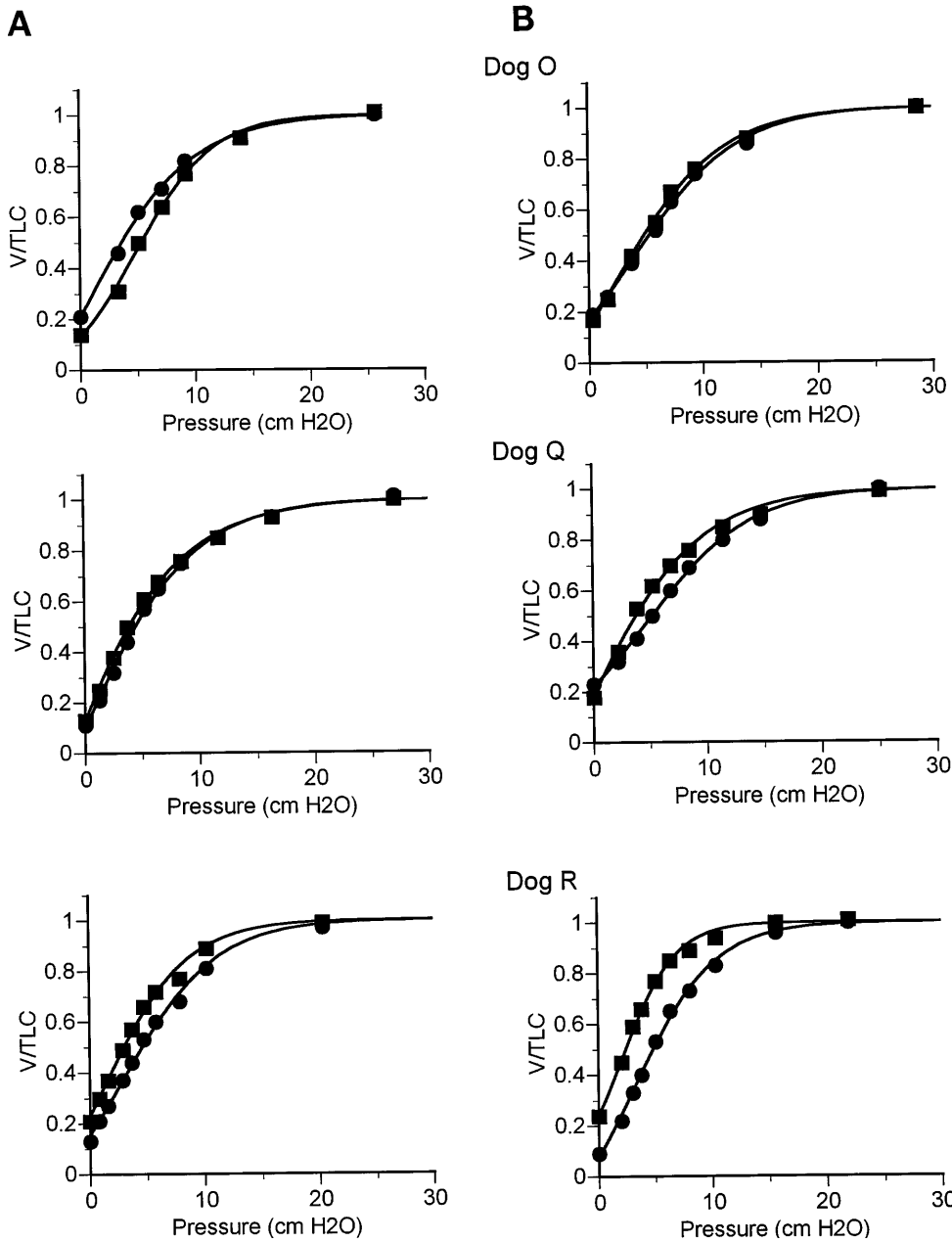


Fig. 6. L (●) and R (■) lung-deflation P-V curves in 3 dogs before LPAO (A) and after LPAO (B).

stated that unilateral PAO caused an increase in resistance and decrease in compliance on the occluded side, with concomitant shift in ventilation away from that side in spontaneously breathing dogs. This effect was prevented by ventilation with 6% CO₂ in air or prior administration of isoproterenol aerosol but not by atropine or vagotomy, implicating a local response to

hypocapnia. Thus, hypocapnic pneumoconstriction is a potential mechanism by which the lung may redistribute ventilation on a local level to optimize ventilation-perfusion matching.

Many investigators have subsequently confirmed or extended these results in other models and in humans. Sterling (19) demonstrated that voluntary hyperventilation in humans to an end-tidal PCO₂ of 25–30 Torr decreased specific airways conductance 37%, an effect blocked by inhaled CO₂ and decreased by atropine. Ingram (4), working in open-chest dogs, found increased lung resistance and decreased compliance with alveolar hypocapnia independent of systemic PCO₂ and vagal reflexes. Other authors have further looked at the effects of local decreases in alveolar PCO₂. Traystman et al. (20, 21) found that lung collateral resistance in-

Table 2. Ventilatory heterogeneity estimates

Condition	<i>r</i> ²		CV, %	
	Left	Right	Left	Right
Control	0.96 ± 0.02	0.96 ± 0.02	12.3	12.3
LPAO	0.95 ± 0.01	0.94 ± 0.02	14.5	16.7

Values are means ± SE; *n* = 12. *r*², correlation coefficient; CV, coefficient of variation.

creased when local PCO_2 decreased, whether that decrease was caused by increased ventilation or decreased blood flow. Kaise et al. (5) modeled this effect and predicted a graded response of collateral resistance to decreasing local PCO_2 as it fell from 5 to 0%. These authors did not measure compliance. This response has further been shown to be independent of atropine, chlorpheniramine, and indomethacin but attenuated by calcium channel blockers (6, 9), β -agonists (6), and K^+ channel openers (8), supporting a locally mediated mechanism.

In a preliminary study (24), we showed that alveolar hypocapnia, with normal systemic blood gases achieved by using ECMO, caused an increase in both the Re and Im parts of whole lung Z over the frequency range 0.5–15 Hz. This effect was greater at lower frequencies, consistent with its having an important role in redistributing ventilation during normal breathing. However, to fully understand the nature of these changes in lung mechanical properties and the mechanism by which they redistribute ventilation, it is important to simultaneously quantify the changes in mechanics, ventilation distribution, and, importantly, V_L . Dynamic positron imaging with radioactive ^{13}N gas (16, 22, 23) is a technique that permits the direct and simultaneous measurement of regional mean and tidal lung volumes, and input Z during unilateral interventions, without restricting their natural distribution.

Methodological considerations. The two-dimensional planar positron-imaging technique used here has been discussed in detail in previous reports (16, 22, 23). The low solubility and short half-life (9.96 min) of radioactive ^{13}N make this gas an ideal tracer for the lung air spaces, and its high energy $[\gamma]$ -emissions are minimally scattered by lung and chest wall tissue. Although tomographic positron imaging shares many of these attributes and additionally provides three-dimensional information, the two-dimensional planar detector is large enough to image the entire lung which, combined with the rapid gated-data collection capabilities, allows dynamic imaging of regional lung volumes.

As discussed previously (16), a potential problem results from the fixed region of interest used to define the R and L lungs. Mediastinal motion may cause lung migration outside or across this boundary, which could cause an error in the $V_{T,r}$ and $V_{L,r}$ values obtained. The open-chest preparation in this experiment would have minimized R-to-L motion of the midline. However, the configuration of the dog's cardiac lobe is such that the tendency is to attribute R-sided tissue to the L lung. Thus, any error from this source would tend to decrease the measured shift in ventilation away from the L lung noted above.

A second potential source of error lies in the assumption that the pneumotachograph flow signal is in phase with the derivative of the whole V_L signal obtained from dynamic imaging. Although a small phase difference between the airway opening and alveolar compartment may exist and thus might slightly alter the decomposition of the impedance into Re and Im parts, the same correction factor was applied to the L and R

lungs. Thus, results expressed as L/R differences or ratios should not be significantly affected.

Finally, to assess the stability of the preparation over the image-collection period, data were collected in three consecutive segments. No differences were found between the $\bar{V}_{L,r}$ or $\bar{V}_{T,r}$ obtained during the shorter first and third segments (the third segment was longer than the first to obtain comparable counts due to radioactive decay). The middle, longest, data collection period was then used for the complete data analysis. Eucapnic ventilation was maintained throughout this data-collection period. Furthermore, there were no differences between $|Z|$ responses from the LPAO₁ and LPAO₂ measurements, suggesting the preparation remained stable over the course of the experiment.

Effects of PAO on ventilation distribution. LPAO with continued ventilation resulted in a marked increase in $|Z_L|$ relative to $|Z_R|$, resulting in a redistribution of ventilation away from the occluded side (Fig. 2 and Table 1). This $|Z|$ increase was due to increases in both Re $\{Z\}$ and Im $\{Z\}$ components (Fig. 3 and Table 1). Due to the difference in absolute magnitudes of the two components and to the defining relationship

$$|Z| = (\text{Re}\{Z\}^2 + \text{Im}\{Z\}^2)^{1/2}$$

the Im $\{Z\}$ accounts for 85–95% of the total $|Z|$ at this frequency. Thus, despite the greater relative increase in Re $\{Z\}$, the V_T redistribution is predominantly due to changes in Im $\{Z\}$. At higher frequencies, the relative contribution of Re $\{Z\}$ increases, but, even at 1 Hz, Im $\{Z\}$ accounts for $\sim 72\%$ of $|Z|$, based on data obtained from closed-chest, normal dogs by using this same technique (15).

A somewhat surprising finding was that the two lungs remained relatively synchronous, with only $\sim 10^\circ$ of phase difference between them in the face of a 230% change in $|Z_r|$ ratio (Fig. 2 and Table 1). That this relative synchrony results from the predominant influence of the Im $\{Z\}$ on the $|Z|$ change can be illustrated by the following calculation. The phase angle ϕ may be calculated for each lung relative to the input as $\phi = \tan^{-1}[\text{Re}\{Z\}/\text{Im}\{Z\}]$. Using the mean Re and Im $\{Z\}$ data from Table 1, the L lung ϕ changes from -14.3 to -25.6° , a change of $\sim 11^\circ$. If the change in $|Z|$ were due entirely to a change in Re $\{Z\}$ [Re $\{Z\} = 72.9$, Im $\{Z\} = -36.4$], then the L lung ϕ after LPAO would be -63.4° , a difference of 49° from control. In contrast, if the entire $|Z|$ change were due to a change in Im $\{Z\}$ [Re $\{Z\} = 9.3$, Im $\{Z\} = -80.9$], then the change in ϕ would be only -7.7° . The degree of asynchrony seen with LPAO would result in <5 ml additional effective V_T due to pendelluft flow between the lungs, calculated by comparing the V_T at the airway opening needed to generate the in-phase component of each lung's V_T to the sum of the actual L and R V_T (13).

These findings are advantageous for a mechanism that functions to regulate the distribution of ventilation on a regional level in response to alterations in local blood flow. At normal breathing frequencies, very large changes in airways resistance can occur without

causing significant alterations in ventilation distribution (16), whereas changes in elastance are most effective in redistributing ventilation in this frequency range (22). Furthermore, the preservation of synchronous regional lung expansion would allow this redistribution of ventilation to occur without causing excessive shear forces between adjacent lung units. This explanation could provide an important physiological role to the observation that E and resistance appear to be linked in such a way that their ratio (η or, alternatively, regional time constants) remains relatively constant over a variety of conditions (3, 11).

$L/R \bar{V}_L$ decreased significantly during LPAO (Fig. 2 and Table 1), reflecting increased recoil of the constricted lung as indicated by the P-V curves (Figs. 5 and 6). Note that the comparisons of the individual lung V_L were not statistically significantly different. This is due to the sensitivity of V_L to small changes in P_{aw} between measurements, an effect corrected for by the L/R ratio. This decreased V_L also reflects the loss of ventilated alveoli caused by airway closure and gas trapping. However, the decrease in V_L cannot account for the observed changes in lung mechanical properties, because sA and sC , two tissue-intensive parameters, both change significantly in the L lung.

The P-V curves show a consistent shift in the L-lung curve to the right after LPAO, indicating an increase in L-lung recoil and stiffness. This increased recoil is present despite the performance of several TLC inflations while equilibrating the lungs for the P-V maneuver. Severinghaus (12) demonstrated that hypocapnic pneumoconstriction was transiently decreased by hyperinflation, and thus one would expect these changes to be underestimates of the steady-state mechanical properties. Nevertheless, these changes indicate a mechanical response of the lung tissue to PAO.

Within each lung, parallel heterogeneity was assessed by analyzing the shape of the washout curves. When multiple compartments wash out in parallel, the whole lung-washout curve becomes multiexponential, and the log-washout curve becomes nonlinear. Modeling this process as a set of 10 compartments having a normal distribution of specific ventilations (sV) with mean \bar{V} and standard deviation σ , the r^2 of the fit of the log-washout curve to a straight line can be correlated to the CV σ/\bar{V} of the multicompartment system (APPENDIX 1). The log-washout curves were extremely linear, indicating a minimum of intraregional heterogeneity. CV for both the control and LPAO lungs were $<17\%$ (Table 2). This compares well to a CV of 15% for ventilatory heterogeneity in closed-chest normal dogs measured with a similar technique (25) and to a CV of $\sim 20\%$ estimated from a variety of data from the literature (26). Importantly, there was no significant change in the CV with LPAO, suggesting that the constriction was relatively uniform or at least did not result in significant ventilatory heterogeneity.

Further evidence that these results reflect changes in tissue properties due to parenchymal smooth muscle constriction may be obtained by analyzing the data according to the structural-damping hypothesis (3).

Although we did not measure tissue resistance (R_{ti}) directly, if one assumes that at low frequency both the contribution of airways resistance to $\text{Re}[Z]$ and parallel heterogeneity are small, R_{ti} may be estimated from the relationship

$$R_{ti} = \eta E_{dyn}/\omega$$

where $E_{dyn} = -\omega \text{Im}[Z]$ and $\eta = \text{Re}[Z]/\text{Im}[Z]$. Partitioning of resistance between airways and tissue in dogs by using alveolar capsules showed that the airways contributed 15 and 11% of lung resistance at 0.5 Hz under control and prostaglandin $F_{2\alpha}$ ($\text{PGF}_{2\alpha}$) constriction, respectively (10). This airways contribution increased to 52 and 47% at 2 Hz. Our washout data suggest that there is not substantial parallel inhomogeneity in this preparation. On the basis of these assumptions, the data showed a 2.3-fold increase in L/R elastance and 2.1-fold increase in η , suggesting roughly equal contributions of E and η to the changes in R_{ti} . These findings are consistent with changes in the mechanical properties of lung parenchymal strips constricted in vitro with various agonists (2), in which different contractile states were characterized by the relative contributions of E_{dyn} and η . Whereas E_{dyn} accounted for at least half of the change in R_{ti} under all conditions, the contributions of E_{dyn} and η were approximately equal for histamine and $\text{PGF}_{2\alpha}$ at the highest concentrations tested (2). Thus, our results are consistent with a constrictive process at the tissue level, and, further, the nature of this process appears similar to that of constriction induced by histamine and $\text{PGF}_{2\alpha}$.

In the intact animal, the presence of the chest wall and interdependence may limit the decrease in V_L with increases in unilateral recoil. In this open-chest animal model, however, the individual lungs are free to change their volumes independently in response to changes in recoil, potentially making these lungs more prone to air trapping as volume falls. Air trapping was measured by comparing the \bar{V}_L after ^{13}N equilibration during tidal breathing, which will give the ventilated V_L , with the \bar{V}_L obtained after tracer equilibration with the use of several TLC inflations. This approach assumes that, even after LPAO, all trapped regions will open up at TLC. LPAO resulted in a variable increase in air trapping in the L lung immediately after the intervention, with further increases in air trapping in both lungs over time (Fig. 4). The P-V curves (Figs. 5 and 6) demonstrate this phenomenon as well. There was a significant correlation ($r = 0.82$, $P < 0.05$) between the degree of air trapping and the change in $|Z|$ in the L lungs. Because the response was not attributable to the changes in ventilating V_L , this correlation may be interpreted to indicate that those lungs which constricted more were also more likely to exhibit airway closure and air trapping. These results underscore the importance of measuring ventilated V_L during interventions that affect lung mechanical properties.

The variability of the response to hypocapnia between animals was also notable. For example, whereas the mean \pm SE R/L ratio of $|Z|$ for all eight dogs was

2.84 ± 0.65 , the range was from 1.51 to 6.92. In several test studies performed in which the lungs were imaged after PAO during a right atrial injection of ^{13}N dissolved in saline, no significant tracer showed up in the LPAO lung, indicating complete occlusion of pulmonary blood flow. We further confirmed PAO each time by the dramatic and immediate blanching of the lung color observed. Thus, we do not believe that incomplete PAO was a cause of this variability. Secondly, we did not pretreat these animals with atropine to block a potential vagal reflex component of the response, because previous authors (4, 6, 12) working in dog models have found that atropine or vagotomy did not diminish the hypocapnic response. There is, however, one study of voluntary hyperventilation in humans in which atropine diminished the increase in airway resistance to the resulting hypocapnia (19). Although we used a deep narcotic anesthetic technique to minimize reflex responses to the highly stimulating surgical procedure, we cannot rule out some degree of variable reflex vagal contribution.

The L and R lungs were not isolated from each other, and thus CO_2 exhaled from the R lung would have been carried into the L lung from the common dead space. This delivery of CO_2 would have tended to decrease the effects of LPAO seen. An additional contributing mechanism may involve the bronchial circulation, which provides an alternate pathway for the delivery of CO_2 and circulating bronchoactive agents to the airways. It is possible that, in the absence of the pulmonary circulation, the bronchial circulation may vary its flow and perhaps even affect the parenchyma. Using radiolabeled microspheres in rabbits, Kowalski et al. (7) found a 50% decrease in bronchial blood flow 60 min after acute PAO; blood flow further decreased to 70% after 4 h. Again, the delivery of CO_2 by the bronchial circulation would only tend to decrease the effects of LPAO, so that the results presented here are conservative. Any circulating substances delivered by the bronchial circulation would be delivered to both lungs, although the absence of pulmonary flow could cause an exaggerated effect. Both of these effects could contribute to the heterogeneity of the responses among dogs. The role of the bronchial circulation in modulating airway responses to hypocapnia and other stimuli is an area of great potential importance.

In summary, we have used dynamic positron imaging to measure the distribution of ventilation, V_L , and lung Z during unilateral PAO in anesthetized, open-chest dogs. PAO results in an increase in the Z_r and a shift in ventilation away from the occluded side, with a minimum of asynchrony between the two lungs. These changes in V_T distribution are attributable to changes in lung compliance that are not solely explained by changes in ventilated V_L and are consistent with a homeostatic mechanism to redistribute regional ventilation in response to changes in blood flow for optimization of ventilation-perfusion matching at normal breathing frequencies.

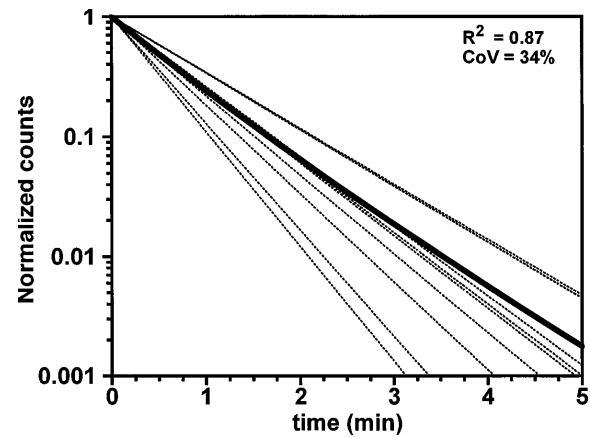


Fig. 7. Example of 10-compartment washout simulation. Dotted lines, individual compartment washout curves; thick line, whole lung-washout curve. Correlation coefficient (R^2) for the whole lung washout was 0.87, corresponding to a coefficient of variation (CoV) for specific ventilation of 34%. See text for details.

APPENDIX 1

Assessing intraregional ventilatory heterogeneity from washout curves. The washout of a tracer gas from a single, uniformly ventilated compartment produces a single exponential washout curve whose time constant τ is inversely related to the ventilation per unit volume [specific ventilation ($s\dot{V}$)]. The presence of ventilatory heterogeneity or multiple parallel compartments results in a multiexponential washout curve or, equivalently, a nonlinear semilog washout curve. The $s\dot{V}$ of this curve can still be measured by using the modified Stewart-Hamilton method and reflects the volume-weighted average of the regional $s\dot{V}$ (17).

We utilized this relationship to model the effect of ventilatory heterogeneity on the linearity of the log-washout curve. The lung was modeled as 10 parallel compartments with the distribution of $s\dot{V}$ among the compartments set such that the mean remained constant and the SD varied to give a range of CV (SD/mean). The 10 washout curves were generated and summed to give the composite washout curve for the entire lung (Fig. 7). This simulated whole lung-washout curve was fit with a log-linear regression and the r^2 of the fit, an index of the linearity of the semilog-washout curve, plotted against the CV of the 10-compartment model distribution. This process was repeated for several sets of $s\dot{V}$, and the results

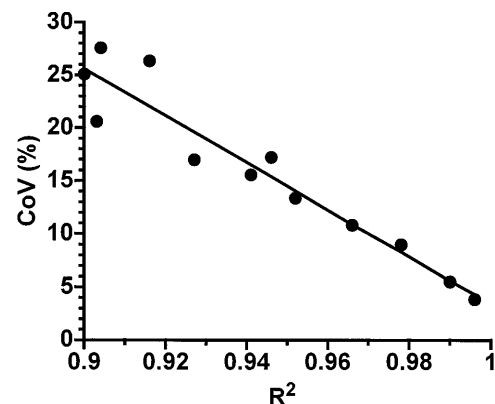


Fig. 8. Relationship of r^2 for log-linear fit of whole lung-washout curve to CoV for specific ventilation for 10-compartment model. Data points were determined from simulation; line is linear regression over these points.

were fitted with a straight line (Fig. 8). The results showed that, as the CV increased, there was increasing departure of the composite log-washout curve from linearity. The data obtained from the control and LPAO washouts correspond to CV values of 12 and 16%, respectively (Table 2), which are comparable to estimates of heterogeneity of ventilation of normal lungs reported in the literature (see DISCUSSION) (25, 26).

APPENDIX 2

Curve-fitting P-V curves. P-V curves are frequently normalized to TLC to facilitate comparisons between different experimental conditions and different animals. However, stepwise P-V curves often do not achieve the same maximum pressure for a variety of experimental reasons that could artifactually affect this normalization. Curve fitting the P-V curves allows TLC to be estimated for each curve at a uniform inflation pressure and, in addition, permits more quantitative comparisons of curves at arbitrary pressure or volume points. We fitted our P-V data to a sigmoidal equation of the form

$$V = A + \frac{B}{1 + e^{-(P-C)/D}}$$

where $V = V_L$, $P = P_{aw}$, and A , B , C , and D are model parameters. This particular equation was chosen because of its ability to closely fit the data rather than any specific meaning of the parameters. A corresponds to the lower asymptote of the sigmoidal curve, and $A + B$ corresponds to the upper asymptote, which was taken as TLC and used to normalize the curves. The fits to the P-V data are shown as the solid lines in Figs. 5 and 6. The r^2 for these fits were all >0.997 ; mean \pm SD r^2 for all fits was 0.997 ± 0.003 . Recoil differences between R and L lungs were calculated from the P_{aw} of the fitted curves at 50% TLC.

This work was supported by National Heart, Lung, and Blood Institute Grant HL-38267 and by the Massachusetts General Hospital Department of Anesthesia.

Address for reprint requests: J. G. Venegas, Dept. of Biomedical Engineering, Clinics 2, Massachusetts General Hospital, Boston, MA 02114.

Received 18 July 1995; accepted in final form 12 November 1996.

REFERENCES

1. **Brownell, G. L., and C. A. Burnham.** Recent developments in positron scintigraphy. In: *Instrumentation in Nuclear Medicine*, edited by G. J. Hine and G. A. Sorenson. New York: Academic, 1974, p. 135-159.
2. **Fredberg, J. J., D. Bunk, E. Ingenito, and S. A. Shore.** Tissue resistance and the contractile state of lung parenchyma. *J. Appl. Physiol.* 74: 1387-1397, 1993.
3. **Fredberg, J. J., and D. Stamenović.** On the imperfect elasticity of lung tissue. *J. Appl. Physiol.* 67: 2408-2419, 1989.
4. **Ingram, R. H., Jr.** Effects of airway versus arterial CO₂ changes on lung mechanics in dogs. *J. Appl. Physiol.* 38: 603-607, 1975.
5. **Kaise, A., A. N. Freed, and W. Mitzner.** Interaction between CO₂ concentration and flow rate on peripheral airway resistance. *J. Appl. Physiol.* 70: 2514-2521, 1991.
6. **Kolbe, J., S. R. Kleeberger, H. A. Menkes, and E. W. Spannhaake.** Hypocapnia-induced constriction of the canine peripheral airways exhibits tachyphylaxis. *J. Appl. Physiol.* 63: 497-504, 1987.
7. **Kowalski, T. F., S. Guidotti, M. Deffebach, P. Kubilis, and M. Bishop.** Bronchial circulation in pulmonary artery occlusion and reperfusion. *J. Appl. Physiol.* 68: 125-129, 1990.
8. **Lindeman, K. S., and A. N. Freed.** Lemakalim attenuates hypocapnia- and dry air-induced bronchoconstriction in canine peripheral airways. *J. Appl. Physiol.* 75: 86-92, 1993.
9. **Lindeman, K. S., C. A. Hirshman, and A. N. Freed.** Calcium channel blockers modulate airway constriction in the canine lung periphery. *J. Appl. Physiol.* 70: 624-630, 1991.
10. **Ludwig, M. S., I. Dreshaj, J. Solway, A. Munoz, and R. H. Ingram, Jr.** Partitioning of pulmonary resistance during constriction in the dog: effects of volume history. *J. Appl. Physiol.* 62: 807-815, 1987.
11. **Ludwig, M. S., F. M. Robatto, S. Simard, D. Stamenović, and J. J. Fredberg.** Lung tissue resistance during contractile stimulation: structural damping decomposition. *J. Appl. Physiol.* 72: 1332-1337, 1992.
12. **Severinghaus, J. W., E. W. Swenson, T. N. Finley, M. T. Lategola, and J. Williams.** Unilateral hypoventilation produced in dogs by occluding one pulmonary artery. *J. Appl. Physiol.* 16: 53-60, 1961.
13. **Simon, B. A.** *The Dynamic Distribution of Pulmonary Ventilation during High-frequency Ventilation* (PhD thesis). Baltimore, MD: Johns Hopkins University, 1987.
14. **Simon, B. A., and W. Mitzner.** Design and calibration of a high-frequency oscillatory ventilator. *IEEE Trans. Biomed. Eng.* 38: 214-218, 1991.
15. **Simon, B. A., K. Tsuzaki, C. A. Hales, and J. G. Venegas.** Ventilation distribution and regional impedance during partial unilateral bronchial obstruction (Abstract). *FASEB J.* 7: A10, 1993.
16. **Simon, B. A., K. Tsuzaki, and J. G. Venegas.** Ventilation distribution and regional lung impedance during partial unilateral bronchial obstruction. *J. Appl. Physiol.* 78: 663-669, 1995.
17. **Simon, B. A., and J. G. Venegas.** Analyzing ¹³NN lung washout curves in the presence of intraregional non-uniformities. *J. Appl. Physiol.* 76: 956-964, 1993.
18. **Simon, B. A., G. G. Weinmann, and W. Mitzner.** Mean airway pressure and alveolar pressure during high-frequency ventilation. *J. Appl. Physiol.* 57: 1069-1078, 1984.
19. **Sterling, G. M.** The mechanism of bronchoconstriction due to hypocapnia in man. *Clin. Sci.* 34: 277-285, 1968.
20. **Traystman, R. J., G. K. Batra, and H. A. Menkes.** Local regulation of collateral ventilation by oxygen and carbon dioxide. *J. Appl. Physiol.* 40: 819-823, 1976.
21. **Traystman, R. J., P. B. Terry, and H. A. Menkes.** Carbon dioxide—a major determinant of collateral ventilation. *J. Appl. Physiol.* 45: 69-74, 1978.
22. **Tsuzaki, K., C. A. Hales, D. J. Streider, and J. G. Venegas.** Regional lung mechanics and gas transport in lungs with inhomogeneous compliance. *J. Appl. Physiol.* 75: 206-216, 1993.
23. **Venegas, J. G., K. Tsuzaki, B. J. Fox, B. A. Simon, and C. A. Hales.** Regional coupling between chest wall and lung expansion during HFV: a positron imaging study. *J. Appl. Physiol.* 74: 2242-2252, 1993.
24. **Venegas, J. G., K. Tsuzaki, D. J. Streider, and C. A. Hales.** Effects of alveolar PCO₂ on respiratory system impedance (Z) (Abstract). *FASEB J.* 5: A4428, 1991.
25. **Venegas, J. G., Y. Yamada, C. Burnham, and C. A. Hales.** Local gas transport in eucapnic ventilation: effects of gravity and breathing frequency. *J. Appl. Physiol.* 68: 2287-2295, 1990.
26. **Wilson, T. A., and K. C. Beck.** Contributions of ventilation and perfusion inhomogeneities to the \dot{V}_A/\dot{Q} distribution. *J. Appl. Physiol.* 72: 2298-2304, 1992.